High strength and ductile low density austenitic FeMnAlC steels: Simplex and alloys strengthened by nanoscale ordered carbides

I. Gutierrez-Urrutia* and D. Raabe

We introduce the alloy design concepts of high performance austenitic FeMnAlC steels, namely, Simplex and alloys strengthened by nanoscale ordered κ-carbides. Simplex steels are characterised by an outstanding strain hardening capacity at room temperature. This is attributed to the multiple stage strain hardening behaviour associated to dislocation substructure refinement and subsequent activation of deformation twinning, which leads to a steadily increase of the strain hardening. Al additions higher that 5 wt-% promote the precipitation of nanoscale $L'1_2$ ordered precipitates (so called κ-carbides) resulting in high strength (yield stress ~1·0 GPa) and ductile (elongation to fracture ~30%) steels. Novel insights into dislocation–particle interactions in a Fe–30·5Mn–8·0Al–1·2C (wt-%) steel strengthened by nanoscale κ-carbides are discussed.

Keywords: Low density steels, High Mn steels, Microstructure control, κ-carbides, Strain hardening, Deformation mechanisms

This paper is part of a special issue on Adventures in the Physical Metallurgy of Steels

Introduction

The development of high performance lightweight steels for structural applications, in particular in the automotive industry, is currently one of the main targets in the steel industry.[1] These steel grades allow the manufacture of lightweight crash resistance car body structures, leading to safer cars and a considerable reduction in fuel consumption and, hence, reduced CO_2 emissions. The FeMnAlC system is a promising low density steel grade that offers a combination of outstanding mechanical properties (yield strength: 0·5–1·0 GPa, ultimate tensile strength: 1·0–1·5 GPa; elongation: 30–80%[1–8]) and specific weight reduction (1·5% density reduction per Al addition of 1 wt-%[2]). Depending on the chemical composition range, these steels can be ferritic (α-phase) (Mn <8 wt-%, Al: 5–8 wt-%, C <0·03 wt-%), austenitic (γ-phase) (Mn: 15–30 wt-%, Al: 2–12 wt-%, C: 0·5–1·2 wt-%) and duplex, i.e. ferritic-+austenitic (Mn: 5–30 wt-%, Al: 3–10 wt-%, C: 0·1–0·7 wt-%). Among these steels, austenitic FeMnAlC alloys are very promising due to their superior mechanical behaviour and simple alloy design. Alloys with low Al content (<5 wt-%) contain single austenite phase at room temperature and exhibit outstanding strain hardening capacity due to their hierarchical deformation structure.[6] Here, we coin these steels as Simplex. The addition of Al promotes the precipitation of nanosized ordered $L'1_2$ $(Fe,Mn)_3AlC$ type carbides (so called κ-carbides) that control the mechanical strength.[9] As these particles contain ordered face centred cubic (fcc) structure, the type of matrix/κ interface is strongly dependent on the matrix structure, i.e. fcc (austenite-γ) or bcc (ferrite-α). In austenitic FeMnAlC steels, γ/κ interfaces are coherent (lattice mismatch <3%[9]), whereas α/κ interfaces in ferritic or duplex steels are semicoherent (lattice mismatch ~6%[10]). As a consequence, at the same aging conditions (<100 h at 600°C), κ-carbides are nanoscale cuboidal precipitates in austenitic FeMnAlC steels,[4,5,8,11,12] whereas in ferritic or duplex steels, these precipitates are thicker and contain elongated rod type shape.[10] It is thus clear that the investigation of dislocation/κ-carbide interaction mechanisms is key to understand the influence of these precipitates on mechanical behaviour. In particular, the few studies devoted so far to the study of these mechanisms in austenitic FeMnAlC steels indicate that particle shearing is the most relevant deformation mechanism.[2,5] The aim of this study is first, to introduce the alloy design concepts of austenitic FeMnAlC steels, namely, Simplex and alloys strengthened by nanoscale ordered κ-carbides, and second, to investigate the underlying deformation mechanisms.

Experimental

The chemical compositions of the investigated steels were Fe–30·5Mn–2·1Al–1·2C and Fe–30·5Mn–8·0Al–1·2C (in wt-%). The materials were melted in an induction furnace under Ar atmosphere and cast to round bars of 25 mm in diameter. The cast ingots were reheated to 1200°C for 30 min, hot rolled to 75% thickness reduction at 1100°C and water quenched. The hot rolled materials were then solution treated for 2 h at 1100°C under Ar, and final water quenching. Subsequent annealing treatments were performed between 450 and 600°C. Tensile tests were carried out at room temperature at an initial strain rate of 5×10^{-4} s^{-1} in a Zwick ZH 100 tensile machine. In

Max-Planck-Institut für Eisenforschung, Max-Planck Str. 1, D-40237 Düsseldorf, Germany

*Corresponding author, email i.gutierrez@mpie.de

Published by Maney on behalf of the Institute
Received 8 October 2013; accepted 22 January 2014
DOI 10.1179/1743284714Y.0000000515

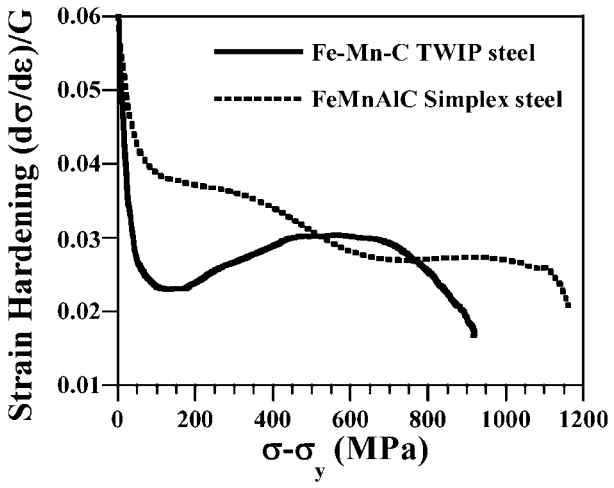

1 Normalised strain hardening rate (normalised with shear modulus) versus flow stress σ subtracted by the yield stress σ_y of Fe–22Mn–0·6C (wt-%) TWIP steel and Fe–30·5Mn–2·1Al–1·2C (wt-%) Simplex steel (deformation conditions: tensile loading at initial strain rate of 5×10^{-4} s^{-1})

addition to tensile testing to failure, interrupted tensile tests to different strain levels were performed to study the microstructural evolution as a function of strain. The tensile samples were cylindrical, with gauges of 6 mm diameter and 40 mm length. Microstructures of the tensile deformed steels were examined by electron channelling contrast (ECC) imaging and transmission electron microscopy (TEM). In all cases, the longitudinal sections were examined, i.e. the observation direction was perpendicular to the tensile axis. ECC observations were performed in a recently developed electron backscatter diffraction based set-up that allows to obtain ECC images under controlled diffraction conditions with enhanced dislocation and interface contrast.[13,14] This approach has been successfully applied to the characterisation of complex deformation structures in steels.[6,15–19] ECC observations were carried out in a Zeiss Crossbeam instrument (XB 1540; Carl Zeiss SMT AG, Germany). TEM observations were conducted in a Phillips CM20 microscope. Thin foil samples were prepared by electropolishing using 30% nitric acid in methanol at −30°C and 10 V.

Results and discussion

FeMnAlC Simplex steels

FeMnAlC Simplex steels are austenitic high Mn steels that are characterised by an outstanding strain hardening capacity at room temperature. This is attributed to the multiple stage strain hardening behaviour associated to dislocation substructure refinement and subsequent activation of deformation twinning, which leads to a steadily increase of the strain hardening.[6] Figure 1 shows the strain hardening curves of a twinning-induced plasticity (TWIP) Fe–22Mn–0·6C (wt-%) steel[16] and a Fe–30·5Mn–2·1Al–1·2C (wt-%) Simplex steel,[6] with similar average grain size (~50 μm). The strain hardening of the TWIP steel exhibits the typical 'hump' associated to the strong microstructure refinement by deformation twinning, the so called TWIP effect.[20–24] This is ascribed to the role of twin interfaces on plasticity and the activation of deformation twinning at low stress levels, close to the yield stress.[25] The good mechanical compatibility between dislocation slip and the evolving twin interfaces results in a critical stress required to transfer plastic deformation across the twin bundle $\tau_{transfer}$, which is only dependent on the shear modulus G and twin thickness t: $\tau_{transfer}\sim Gb/t$ (b: magnitude of the Burgers vector).[26] In particular, this stress is higher than that required to transfer plasticity across a dislocation boundary with low misorientation, $\tau_{transfer}\sim G(\theta/Db)^{1/2}$ (D: dislocation substructure size, θ: misorientation angle).[27] Taken into account that deformation twins in high–Mn steels contain nanosized thicknesses (typically <100 nm[6,16,24]), a relatively small twin volume fraction is required to enable the TWIP effect. As the twin spacing is the key microstructural parameter, hence, twinning kinetics determine the mechanical properties in TWIP steels.

Figure 2 shows ECC images of the deformation structures in a Fe–30·5Mn–2·1Al–1·2C (wt-%) Simplex steel tensile deformed to 0·1 true strain/710 MPa (Fig. 2*a*), 0·2 true strain/950 MPa (Fig. 2*b*) and 0·3 true strain/1150 MPa (Fig. 2*c* and *d*). This figure reveals the gradual microstructure refinement by the evolving dislocation and twin substructures. At the early stages of deformation (true strain <0·1), the dislocation substructure is mainly formed by planar dislocation substructures such as Taylor lattices (Fig. 2*a*). With further straining, the planar dislocation substructure evolves into dislocation cells and cell blocks (Fig. 2*b*). The subsequent activation of deformation twinning at ~1 GPa, results in a further microstructure refinement (Fig. 2*c*–*d*) due to the small mechanical resistance that dislocation boundaries have against twin boundaries that cut through them.[16] Figure 2 reveals that in the FeMnAlC Simplex steel, the additions of high carbon content (~1 wt-%) and aluminium (2·1 wt-%) result in a pronounced effect on the deformation structure. This can be explained as follows. Carbon solute has a strong influence on dislocation cross-slip in fcc metals.[28,29] Owing to the strong interaction between edge dislocation components and carbon solute, the constriction energy of cross-slip is high and hence, its frequency is reduced. As cross-slip is a stress-assisted phenomenon, its frequency increases with the applied macroscopic stress.[30] This effect results in the formation of a hierarchical nanosized dislocation substructure that gradually evolves from planar (Taylor lattices) to wavy substructures (cells and cell blocks) (Fig. 2). This dislocation transition is critical to minimising damage mechanisms triggered by local stress concentrations at grain boundaries provided by dense planar dislocation configurations. On the other hand, the addition of aluminium increases the stacking fault energy shifting the activation of deformation twinning to higher stress levels. The development of a hierarchical dislocation substructure and the subsequent activation of deformation twinning results in a multiple stage strain hardening behaviour. As a consequence, the FeMnAlC Simplex steel exhibits a superior combination of strength and ductility than FeMnC TWIP steels.

FeMnAlC steels strengthened by nanoscale ordered κ-carbides

Precipitation state

These alloys are austenitic (γ-phase) steels that contain intragranular nanosized ordered carbides (so called

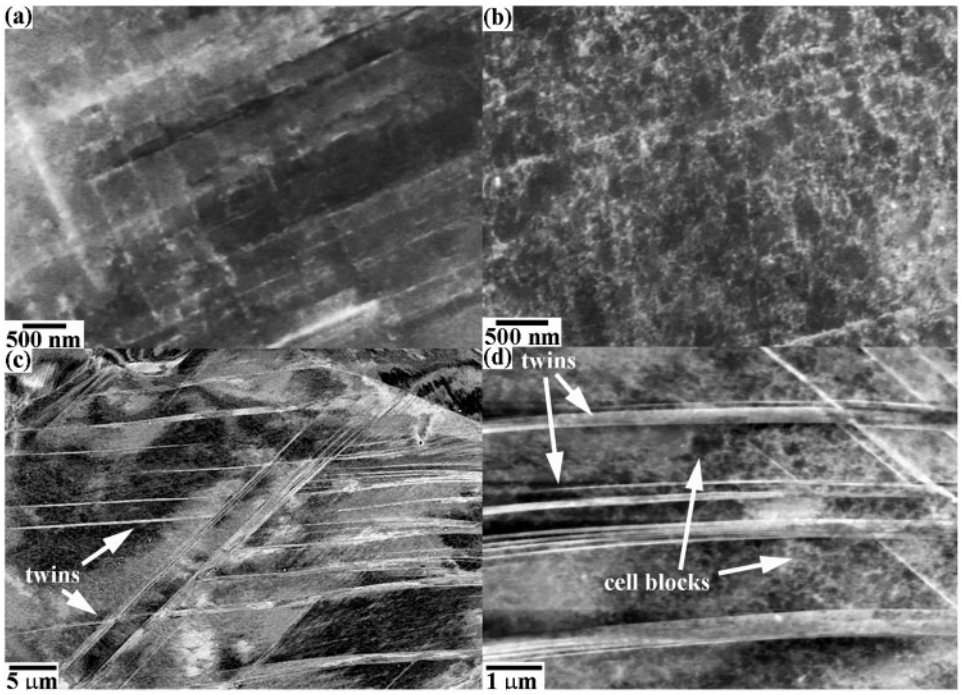

2 ECC images of deformation structures in Fe–30·5Mn–2·1Al–1·2C (wt-%) Simplex steel tensile deformed to *a* 0·1 true strain/710 MPa, *b* 0·2 true strain/950 MPa and *c*, *d* 0·3 true strain/1150 MPa

κ-carbides) at short annealing conditions (<24 h at 550–600°C). With further annealing, grain boundary precipitation occurs which is strongly dependent on alloying content.[11,12] Figure 3 shows dark field TEM images of intragranular κ-carbides in a Fe–30·5Mn–8·0Al–1·2C (wt-%) steel aged at 600°C for 24 h (Fig. 3*a*) and 96 h (Fig. 3*b*). Analysis of selected area diffraction patterns indicates that these precipitates contain a $L'1_2$ type structure with a cube/cube orientation relationship with the austenite matrix. These fcc ordered nanoprecipitates can be identified by the presence of superlattice spots in the corresponding diffraction pattern, as shown in the inset of Fig. 3*a*. Although the exact chemical composition of these carbides is at the moment unknown (detailed carbide characterisation by atom probe tomography is currently undertaken), these carbides are $(Fe,Mn)_3AlC$ type precipitates.[31–35]

In the present annealing conditions, κ-carbides contain two main morphologies, namely, {001} faceted cuboidal (Fig. 3*a*) and plate shaped aligned along the elastically soft <100>-type directions (Fig. 3*b* and *c*). This precipitate morphology is similar to that reported in the γ (fcc)/γ′ ($L1_2$) system in Ni and Co based superalloys.[36] Specifically, at 24 h/600°C, κ-carbides mainly consist of

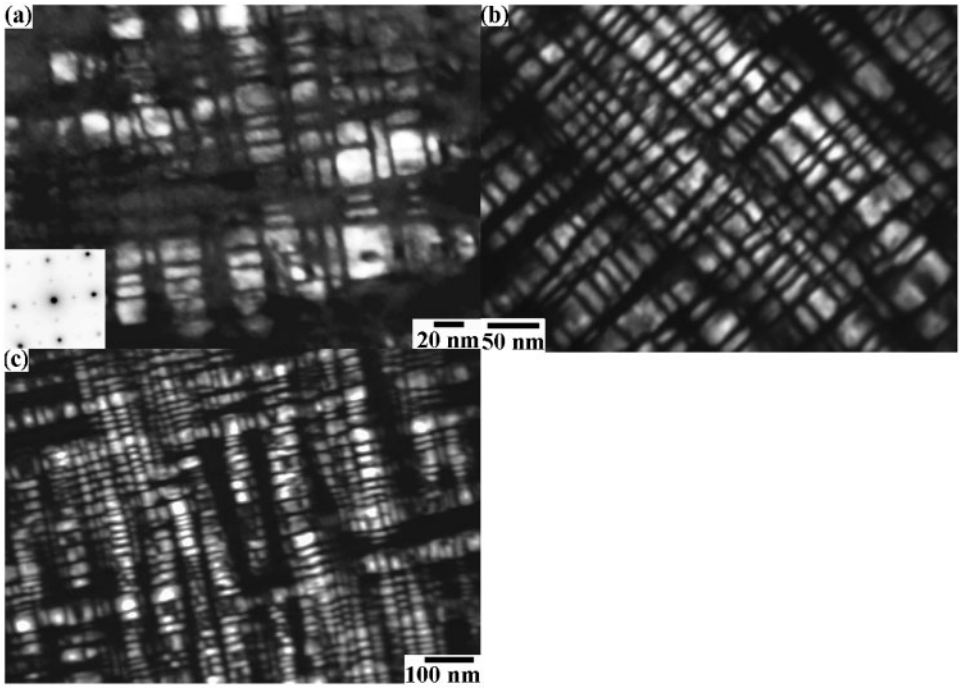

3 Dark field TEM images of κ-carbides in Fe–30·5Mn–8·0Al–1·2C (wt-%) steel aged at 600°C for *a* 24 h and *b*, *c* 96 h

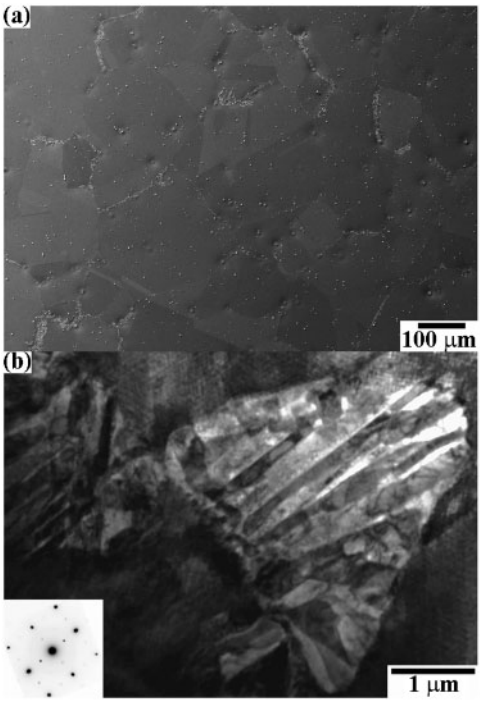

4 *a* SE-SEM image of grain boundary precipitate distribution and *b* BF-TEM image of grain boundary precipitates in Fe–30·5Mn–8·0Al–1·2C (wt-%) steel aged at 600°C for 96 h: diffraction pattern corresponds to both austenite and grain boundary precipitates

cuboids with rounded corners. Their average size is about 20 nm. Some plate shaped carbides with average size of 19×7 nm are also visible. With further aging (96 h/600°C), κ-carbides contain a non-equiaxed rectangular parallel epipedic morphology with an average size of 30×20 nm. Plate type particles contain an average size of 35×8 nm. At this annealing condition, κ-carbides are not distributed homogeneously, they are, however, arranged into rods of 200–500 nm in length that are aligned along <100> type directions (Fig. 3*c*). The interparticle spacing in the rod interior is about 2–5 nm and the spacing between rods is about 30–40 nm.

Grain boundary precipitation was mainly observed for aging times longer than 24 h at 600°C. Figure 4*a* shows a secondary electron SEM image of the distribution of grain boundary (GB) precipitates for an aging time of 96 h. This figure reveals that at this aging condition, grain boundary precipitation is significant. GB precipitates were characterised by TEM (Fig. 4*b*). Analysis of selected-area diffraction patterns indicates that these precipitates are $L'1_2$ κ-type carbides. No indication of ferrite formation was found. This finding agrees with previous reports on GB precipitation in similar FeMnAlC alloys.[11,12] In particular, Hwang *et al.*[12] reported that the chemical composition of intergranular κ-precipitates at an aging temperature of 550°C in an Fe–8·0Al–31·5Mn–1·05C (wt-%) steel is close to the stoichiometric composition, namely, $(Fe,Mn)_3AlC$. Interestingly, the high carbon content is key to delay the formation of the brittle β-Mn intermetallic. Chao *et al.*[11] reported the formation of this intermetallic in an Fe–7·8Al–31·7Mn–0·54C (wt-%) steel aged at 550°C for 90 h. In this alloy, the formation of the very energetically stable intergranular κ-precipitate results in a very carbon-poor austenitic matrix enabling the transformation γ to (β-Mn).

Deformation mechanisms

These austenitic steels strengthened by nanoscale ordered carbides contain high yield strength (0·8–1·2 GPa[1,5,8,9]) and good ductility (elongation: 30–50%[1,5,8,9]). As shown in a previous work,[8] at the aging conditions studied here, intragranular nanosized κ-carbides determine the yield strength (~1 GPa at 24 h/600°C[8]), whereas intergranular κ-carbides control fracture behaviour. Figure 5*a* shows a bright field TEM image of the dislocation substructure of a Fe–30·5Mn–8·0Al–1·2C (wt-%) steel aged at 600°C for 24 h and strained to 0·15 true strain. This image reveals that planar dislocation substructures consisting of dense dislocation arrays spaced between 100 and 300 nm are formed upon straining. This observation indicates that plasticity is mainly concentrated within the dislocation boundaries of such substructures. Figure 5*b–d* show weak beam images of dislocation–particle interactions at different areas of a grain oriented close to <001>// tensile axis direction. These images reveal that at the present deformation conditions, several dislocation-particle interaction mechanisms are active.

Figure 5*b* illustrates dislocation–particle interactions in an area delimited by the dislocation arrays. The main characteristics revealed in this figure are first, an Orowan bypassing mechanism is active, and second, dislocations are held at γ/κ interfaces. Owing to the extremely small interparticle spacing (2–5 nm) dislocations can not bypass κ-carbides individually (σ_{Orowan} about 5–15 GPa with particle size of 20 nm). However, they can bypass the rods containing the nanosized carbides. If we consider the spacing between rods (30–40 nm) it yields σ_{Orowan} about 0·9–1·4 GPa, which is close to the macroscopic stress of 1·3 GPa at 0·15 true strain.[8] Expanding loops along {111} slip planes intersect {100} γ/κ interfaces. As the loops expand through the narrow matrix channels between rods, segments of mixed or edge character are held at the interface while the screw segments may undergo cross-slip and continue to glide. The high stacking fault energy of the Fe–30·5Mn–8·0Al–1·2C (wt-%) alloy (~85 mJ m^{-2} using a modified Olson–Cohen thermodynamical model[37,38] and thermodynamical data available for the FeMnAlC system[39–42]) enables the activation of dislocation cross-slip at γ/κ interfaces. This deformation mechanism has been reported in Ni based superalloys with high volume fraction of γ′ precipitates deformed at low temperatures.[43]

Figure 5*c* illustrates dislocation–particle interactions within a dislocation bundle forming the planar dislocation arrangements shown in Fig. 5*a*. Elongated dislocation segments are observed, which follow the channels of the austenitic matrix. Some of these dislocation contrasts correspond to dislocation dipoles (indicated by arrows). This figure also reveals that some matrix channels seem to contain several superimposed dislocations contrasts, indicating that several successive loops have propagated through them. Figure 5*d* shows a detail of a shear band as a result of localised shear. The projections of the dislocation lines are along <211> directions that correspond to the glide of <101> screw dislocations. The fact that the slip traces are longer than the precipitate size indicates that precipitate shearing necessarily took place. This figure also reveals alignments

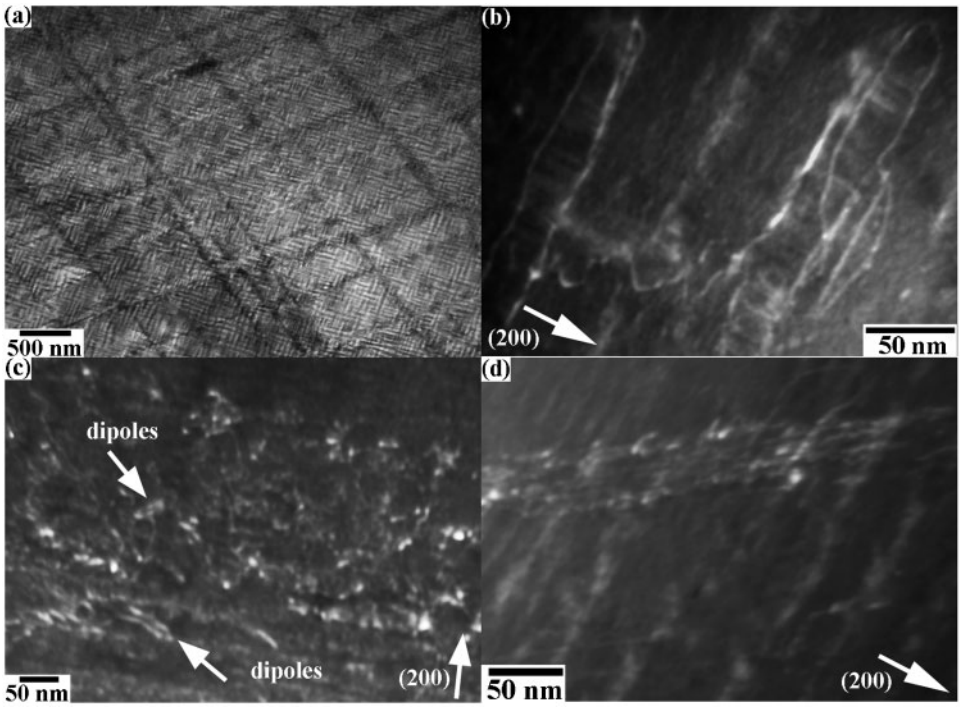

5 *a* TEM image of planar dislocation arrangements and *b–d* weak beam TEM images of dislocation/κ-carbides interactions in Fe–30·5Mn–8·0Al–1·2C (wt-%) steel aged at 600°C for 24 h and tensile deformed to 0·15 true strain: diffraction vectors are indicated by arrows

of dislocation debris contrast in the projections of the <100> channel directions, which underline the contours of the ordered precipitates.

The formation of planar dislocation substructures in FeMnAlC steels strengthened by nanosized κ-carbides has been attributed to the glide softening phenomenon associated with short-range ordering in the solid solution state[44,45] or to the shearing of κ-carbides.[2,5] The present observations indicate that at the current deformation conditions and κ-carbide morphology, size and distribution, the predominant deformation mechanisms are Orowan bypassing of rods of κ-carbides and subsequent expansion of dislocation loops assisted by cross-slip and, to a less extent, shearing of κ-carbides. We suggest that the higher dislocation density localised within dislocation bundles can be associated to differences in the spacing between rods, tending the dislocations to follow preferential paths within the widest ones and even to shear κ-carbide interfaces. This finding underlines the complex dislocation/κ interface interactions occurring in these alloys and provides new insights into the deformation mechanisms of FeMnAlC steels strengthened by nanoscale ordered carbides. Further investigations are required to study the role of size and distribution of κ-carbides on deformation mechanisms and hence, on mechanical behaviour of these materials.

Conclusions

We investigate the deformation mechanisms and strain hardening behaviour of high performance austenitic FeMnAlC steels, namely, Simplex and alloys strengthened by nanoscale ordered κ-carbides. FeMnAlC Simplex steels are characterised by an outstanding strain hardening capacity associated to dislocation substructure refinement and subsequent activation of deformation twinning, which leads to a steadily increase of the strain hardening. FeMnAlC steels strengthened by nanoscale ordered κ-carbides exhibit high strength (yield stress 0·8–1·2 GPa) and good ductility (elongation: 30–50%). Dislocation–κ-carbide interactions analysed by weak beam TEM reveal that at the current deformation conditions and κ-carbide morphology, size and distribution, the predominant deformation mechanisms are Orowan bypassing of rods of κ-carbides and subsequent expansion of dislocation loops assisted by cross-slip and, to a less extent, shearing of κ-carbides.

References

1. H. Kim, D.-W. Suh and N. J. Kim: *Sci. Technol. Adv. Mater.*, 2013, **14**, 014205.
2. G. Frommeyer and U. Brüx: *Steel Res. Int.*, 2006, **77**, 627–633.
3. J. D. Yoo and K.-T. Park: *Mater. Sci. Eng. A*, 2008, **A496**, 417–424.
4. K. M. Chang, C. G. Chao and T. F. Liu: *Scr. Mater.*, 2010, **63**, 162–165.
5. K. Choi, C.-H. Seo, H. Lee, S. K. Kim, J. H. Kwak, K. G. Chin, K.-T. Park and N. J. Kim: *Scr. Mater.*, 2010, **63**, 1028–1031.
6. I. Gutierrez-Urrutia and D. Raabe: *Acta Mater.*, 2012, **60**, 5791–5802.
7. S. Y. Han, S. Y. Shin, H.-J. Lee, B.-J. Lee, S. Lee, N. J. Kim and J.-H. Kwak: *Metall. Mater. Trans. A*, 2012, **43A**, 843–853.
8. I. Gutierrez-Urrutia and D. Raabe: *Scr. Mater.*, 2013, **68**, 343–347.
9. Y. Kimura, K. Handa, H. Hayashi and Y. Mishima: *Intermetallics*, 2004, **12**, 607–617.
10. J.-B. Seol, D. Raabe, P. Choi, H.-S. Park, J.-H. Kwak and C.-G. Park: *Scr. Mater.*, 2013, **68**, 348–353.
11. C. Y. Chao, C. N. Hwang and T. F. Liu: *Scr. Metall. Mater.*, 1993, **28**, 109–114.
12. C. N. Hwang, C. Y. Chao and T. F. Liu: *Scr. Metall. Mater.*, 1993, **28**, 263–268.
13. I. Gutierrez-Urrutia, S. Zaefferer and D. Raabe: *JOM*, 2013, **65**, 1229–1236.
14. I. Gutierrez-Urrutia, S. Zaefferer and D. Raabe, *Scr. Mater.*, 2009, **61**, 737–740.
15. I. Gutierrez-Urrutia and D. Raabe: *Scr. Mater.*, 2012, **66**, 992–996.
16. I. Gutierrez-Urrutia and D. Raabe: *Acta Mater.*, 2011, **59**, 6449–6462.

17. I. Gutierrez-Urrutia and D. Raabe: *Scr. Mater.*, 2012, **66**, 343–346.
18. A. Eisenlohr, I. Gutierrez-Urrutia and D. Raabe: *Acta Mater.*, 2012, **60**, 3994–4004.
19. I. Gutierrez-Urrutia and D. Raabe: *Scr. Mater.*, 2013, **69**, 53–56.
20. O. Bouaziz, S. Allain and C. Scott: *Scr. Mater.*, 2008, **58**, 484–487.
21. H. Beladi, I. B. Timokhina, Y. Estrin, J. Kim, B. C. D. Cooman and S. K. Kim: *Acta Mater.*, 2011, **59**, 7787–7799.
22. H. K. Yang, Z. J. Zhang and Z. F. Zhang: *Scr. Mater.*, 2013, **68**, 992–995.
23. D. Barbier, N. Gey, S. Allain, N. Bozzolo and M. Humbert: *Mater. Sci. Eng. A*, 2009, **A500**, 196–206.
24. O. Bouaziz, S. Allain, C. P. Scott, P. Cugy and D. Barbier: *Curr. Opin. Solid State Mater. Sci.*, 2011, **15**, 141–168.
25. I. Gutierrez-Urrutia, S. Zaefferer and D. Raabe: *Mater. Sci. Eng. A*, 2010, **A527**, 3552–3560.
26. J. W. Christian and S. Mahajan: *Prog. Mater. Sci.*, 1995, **39**, 1–157.
27. D. A. Hughes and N. Hansen: *Acta Mater.*, 2000, **48**, 2985–3004.
28. S. D. Andrews, H. Sehitoglu and I. Karaman: *J. Appl. Phys.*, 2000, **87**, (5), 2194–2203.
29. K. Sekido, T. Ohmura, L. Zhang, T. Hara and K. Tsuzaki: *Mater. Sci. Eng. A*, 2011, **A530**, 396–401.
30. W. Püschl: *Prog. Mater. Sci.*, 2002, **47**, 415–461.
31. C. N. Hwang, C. Y. Chao and T. F. Liu: *Scr. Metall. Mater.*, 1993, **28**, 263–268.
32. K. Sato, Y. Inoue and K. Tagawa: *Metall. Trans. A*, 1988, **21A**, 5–11.
33. K. H. Han, J. C. Yoon and W. K. Choo: *Scr. Metall.*, 1986, **20**, 33–36.
34. S. C. Tjong: *Mater. Char.*, 1990, **24**, 275.
35. K. Sato, K. Tagawa and Y. Inoue: *Metall. Trans. A*, 1990, **21A**, 5–11.
36. R. C. Reed: 'The superalloys: fundamentals and applications'; 2006, New York, Cambridge University Press.
37. S. Allain, J. P. Chateau, O. Bouaziz, S. Migot and N. Guelton: *Mater. Sci. Eng. A*, 2004, **A387**–**A389**, 158–162.
38. A. Dumay, J. P. Chateau, S. Allain, S. Migot and O. Bouaziz: *Mater. Sci. Eng. A*, 2008, **A483**–**A484**, 184–187.
39. J. D. Yoo and K. T. Park: *Mater. Sci. Eng. A*, 2008, **A496**, 417–424.
40. Y.-K. Lee and C.-S. Choi: *Metall. Mater. Trans. A*, 2000, **31A**, 355–360.
41. G. B. Olson and M. Cohen: *Metall. Trans. A*, 1976, **7A**, 1897–1904.
42. J.-E. Jin and Y.-K. Lee: *Acta Mater.*, 2012, **60**, 1680–1688.
43. L. P. Kubin, B. Lisiecki and P. Caron: *Philos. Mag. A*, 1995, **71A**, 991–1009.
44. K.-T. Park, K. G. Jin, S. H. Han, S. W. Hwang, K. Choi and C. S. Lee: *Mater. Sci. Eng. A*, 2010, **A527**, 3651–3661.
45. K.-T. Park: *Scr. Mater.*, 2013, **68**, 375–379.